RSC Advances

PAPER

View Article Online
View Journal | View Issue

Cite this: *RSC Adv.*, 2020, **10**, 18543

Atomic and electronic structures of charge-doping VO_2: first-principles calculations

Lanli Chen, [ab] Yuanyuan Cui,[b] Hongjie Luo[b] and Yanfeng Gao [*bc]

Received 16th March 2020
Accepted 6th May 2020

DOI: 10.1039/d0ra02420a

rsc.li/rsc-advances

The atomic and electronic structures of charge-doping VO_2 are investigated by using first-principles calculations. Hole doping is more conducive to stabilizing the structure of VO_2 than electron doping. The controllable phase transition temperature is coupled with changes in atomic and electronic structures. With the increase in hole density, the V–V chains and twisting angle experience a dramatic change, and the band gap (0.69–0 eV) is rapidly reduced due to orbital switching between the $d_{x^2-y^2}$ and d_{z^2}/d_{yz} orbitals. However, as the electron density increases, the band gap (0.69–0.502 eV) narrows slightly, while the V–O bond lengths significantly increase. The current results provide up a variable way to tune the VO_2 phase transition temperature through charge-doping.

1. Introduction

Vanadium dioxide (VO_2) is an attractive thermochromic material due to its reversible metal–insulator transition (MIT) from a high-temperature rutile phase (R) to a low-temperature monoclinic phase (M) at a phase transition temperature (T_c) of about 68 °C. Across the MIT, VO_2 exhibits a dramatic change in its electrical and optical properties.[1] Therefore, VO_2 is not only attracting wide scientific interest but also has great technological applications in optoelectronic devices,[2,3] sensors,[4] and smart windows.[5–7]

Given the diverse potential applications for VO_2, modulation of the phase transition behavior and decreasing the T_c close to room temperature are the main hottest topics in VO_2 researches. The control of phase transition in VO_2 was successfully implemented with multiple ways including doping,[8,9] point defects,[10,11] external strain,[12] electric fields,[13] and surface and interface engineering.[14] In most of these modulations, doping was proposed to play a strong role in mediating the phase transition temperature of VO_2. Recently, it is reported that charge-doping could effectively decrease the T_c of VO_2. What's the effect of the two types of charge injection, *i.e.* the hole or electron injection, on the tuning the MIT of VO_2? For example, Zhang *et al.*[15] found that the reduction of the T_c is essentially ascribed to the charge injection as the dopants by the first-principles calculations. The surface adsorption of F_4TCNQ molecules assists the phase transition of VO_2 film due to the surface charge transfer.[16] Substitution N-doping or interstitial N-doping in VO_2 allows for a significant reduction in the phase transition temperature from 80.0 to 62.9 °C.[17] Zhang *et al.* also found that the T_c of the metal–insulator transition process decreases with a value of ~18 °C for N-incorporated VO_2 thin films, and the narrowing of the charge doping results in the attenuation of the interaction within the V–V dimer in the M1 phase.[18] Dai *et al.* reported that 2.93% F-doped VO_2 foil exhibits an increased solar-heat shielding ability (35.1%), excellent solar modulation ability (10.7%) and appropriate visible transmittance (48.7%).[19] On the other hand, the incorporation of electrons in the VO_2 lattice could also induce its metal–insulator transition.[20–22] For example, NH_3 can act as a reductant to inhibit the over-oxidization of VO_2, resulting in inferior thermochromic properties.[20] Boron at the interstitial site provides three electrons, and thus, boron doping of VO_2 could drastically reduce the T_c at a rate as large as 31.5 °C per at% B.[21] According to recent theoretical predictions, T_c can be reduced by 27 K per at% W at the GGA+*U* level or by 18.6 K per at% W at the HSE06 level, which is attributed to W-doping providing three electrons and inducing a large structural distortion in the lattice.[22] Actually, the electron or hole-injection in VO_2 is implemented through these concrete methods such as the doping of N, B, F and other metals. For instance, from the point view of the semiconductor doping process, the W atom has one more valence electron than the V atom, so one W atom substituting for a V atom in VO_2 injects only one additional electron into the compound, whereas a B atom which possess two valence electrons in the 2s orbital at an interstitial site can inject its two 2s electrons into the VO_2. In addition, the N is widely considered to be the most promising p-type dopant due to its similar size to oxygen, resistance to forming AX centers.[18] The F atom leads to the loss of the V^{4+}–V^{4+} pairs, as electrons from the donors are injected into the V-3d valence band, resulting in the formation of V^{4+}–V^{3+} pairs *via* charge transfer.[19] Experimentally, Andreev *et al.* observed that hydrogen atoms penetrated into the VO_2 film during thermal decomposition could lead to a lowered phase transition temperature.[23]

[a]*School of Mathematics and Physics, Hubei Polytechnic University, Huangshi 435003, China*

[b]*School of Materials Science and Engineering, Shanghai University, Shanghai 200444, China. E-mail: yfgao@shu.edu.cn*

[c]*Faculty of Chemical Engineering, Huaiyin Institute of Technology, Jiangsu 223003, China*

The above experimental and theoretical results indicate that the T_c and phase transition behavior of VO_2 can be effectively controlled by charge doping. However, the role of type of charge on the reduced phase transition temperature is still a debate and remains to be settled. Therefore, it is of vital importance to reveal the underlying mechanism on the effects of charge-doping on the phase transition behavior for realizing the rational tuning of the phase transition temperature.

2. Computational details

The calculations were conducted with the Vienna *ab initio* simulation package (VASP).[24,25] The potentials were of the projector augmented wave type (PAW) type, and the exchange-correlation part of the density functional was treated within the generalized gradient approximation (GGA) of Perdew–Burke–Ernzerhof (PBE).[26,27] Given the strong on-site Coulomb repulsion among the V-3d electrons, the Hubbard parameter U was added to the PBE functional.[28] As discussed in ref. 9 and 10 the value was chosen as 3.4 eV in the PBE+U formalism. The valence electron configurations for V ($3d^3 4s^2$) and O ($2s^2 2p^4$) atoms were used in the calculations. 530 eV was used as the plane-wave cut-off energy. The Brillouin zone sampling mesh parameters for the k-point set were chosen as $5 \times 5 \times 5$ for the electronic structures. These parameters were used to ensure a total energy converges of 1×10^{-5} eV per unit cell and a maximum force of 0.01 eV $Å^{-1}$. The charge density was tuned by changing the total number of electrons in the unit cell, with a compensating jellium background of opposite charge added or subtracted.[29]

The formation enthalpy of pristine or charge-doped VO_2 was calculated as

$$\Delta H_f = E_{tot}(VO_2) - E_V(\text{bulk}) - 2E\left(\frac{1}{2}O_2\right) \quad (1)$$

where ΔH_f is the formation enthalpy of pristine or charge-doped VO_2. E_V (bulk) is the chemical potential of V in the bulk phase. $E\left(\frac{1}{2}O_2\right)$ is the total energy of the oxygen molecules.

The phase transition temperature (T_c) can be quantitatively calculated *via*[30]

$$T_c = T_{c,0}\frac{\Delta H}{\Delta H_0} \quad (2)$$

where $T_{c,0}$ is the transition temperature of pure VO_2 and a value of 340 K is adopted from ref. 2. ΔH and ΔH_0 are the enthalpy changes associated with the phase transition for doped and pure VO_2, respectively. The enthalpy is approximated as the Helmholtz free energy, which can be obtained from our DFT calculations by neglecting the pV term for condensed matter and omitting the entropy contribution at 0 K.

As shown in Fig. 1(a and b), the basic calculations were performed in the supercells with $2 \times 2 \times 2$ and $2 \times 2 \times 4$ primitive unit cells for VO_2(M) and VO_2(R) phases, respectively. Table 1 lists the calculated structural parameters. The theoretical lattice parameters obtained in this work are in good agreement with the previously reported experimental data.[31]

3. Results and discussion

3.1 Charge induced phase transition for VO_2

Fig. 2(a and b) shows the total energies (E_{tot}) of charge doping in M and R phase as a function of charge density. It can be found that the total energies of charge-doping M phase VO_2 are gradually lower than those of R phase as the charge doping increases, indicating that it is more difficult to obtain R phase VO_2 than the M phase under current conditions. The similar results have been also appeared in electron-injection in two-dimensional transition metal dichalcogenides.[32] Fig. 2(c and d) shows the formation enthalpy of charge-doped VO_2. The trend of the formation enthalpy of electron doping and that of hole doping are contrary. The formation enthalpy of VO_2 linearly increased with the increase in electron density, while the formation enthalpy of VO_2 decreased with the increase in hole density. In addition, hole doping system is more negative than the pristine one, and the electron doping system is less negative than the pristine one, suggesting that hole doping system is more stable than the electron doping. Thus, we conclude that

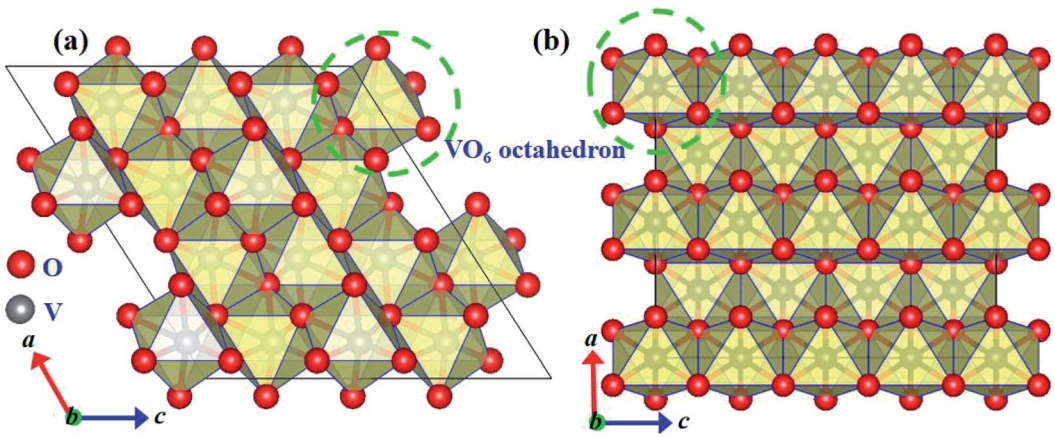

Fig. 1 Crystalline structures of monoclinic (a) and rutile (b) phases of VO_2. V and O atoms are represented by gray and red spheres, respectively.

Table 1 Lattice parameters of pristine VO_2(M) and VO_2(R)

Systems	a (Å)	b (Å)	c (Å)	α (°)	β (°)	γ (°)	V (Å^3)	Ref.
VO_2(M)	5.743	4.517	5.375	90	122.6	90	117.466	Exp.[31]
VO_2(M)	5.626	4.637	5.454	90	121.704	90	121.021	This calc.
VO_2(R)	4.552	4.552	2.852	90	90	90	59.095	Exp.[31]
VO_2(R)	4.652	4.652	2.789	90	90	90	60.336	This calc.

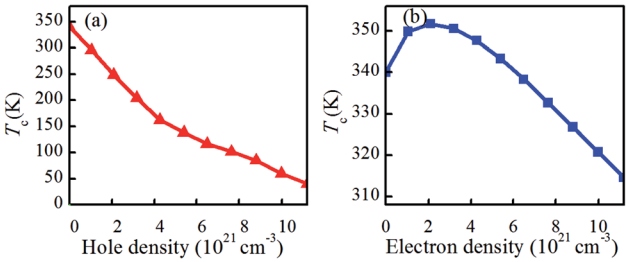

Fig. 3 Dependence of the phase transition temperature (T_c) in VO_2 on the charge density. (a) Hole-doping, and (b) electron doping.

hole doping is more conducive to stabilize the structure of VO_2 than electron doping. This phenomenon has been found in IIA element doping of VO_2(M).[9] Zhang *et al.* reported that the introduction of some electrons in VO_2 *via* W doping results in the instability of the structure.[22]

The dependence of T_c on the charge doping concentration is presented in Fig. 3(a and b). As shown in Fig. 3(a), the T_c of VO_2 is found to be almost linearly proportional to the hole-doping density. It is clearly shown that when the hole density is set at 4.28×10^{21} cm^{-3}, the phase transition of VO_2 could take place at 162.44 K, which is lower than the room temperature of 298 K. This observation is consistent with the experimental observation that hole doping could trigger the MIT below 340 K.[17] Wan *et al.* reported that the reduced phase transition temperature for hole doped VO_2 is due to the fact that hole doping modifies the V-3d orbital occupancy and thus weakens the electron–electron correlation, lowering the crystalline stability energy.[17] Dai *et al.* found that F-doping can effectively decrease the T_c to 35 °C at 2.93% F in VO_2 and that F-doping VO_2 smart glass foils exhibit excellent thermochromism in the near-infrared region.[19] However, the situation for electron-doping is not the same as that of hole-doping. As shown in Fig. 3(b), when the electron density increases from 0 to 2.1×10^{21} cm^{-3}, T_c gradually increases. However, once the electron density is greater than 2.1×10^{21} cm^{-3}, T_c rapidly decreases. For example, an electron density of 2.1×10^{21} cm^{-3} corresponds to a ΔT_c of 11.72 K for electron-doped VO_2, *i.e.*, the phase transition from the rutile phase to the monoclinic phase occurs at 351.72 K. However, an electron density of 1.12×10^{22} cm^{-3} will result in a ΔT_c as large as −25.32 K, implying the reduction in T_c to 314.68 K. Actually, the T_c is related with the charge concentration. In the range of charge concentration, the T_c is almost linearly proportional to the charge density. Experimentally, when cooled down to 120 K, H_xVO_2 ($x > 4\%$) films exhibit metallic properties, and the ΔT_c was around −55 K per at% H.[23]

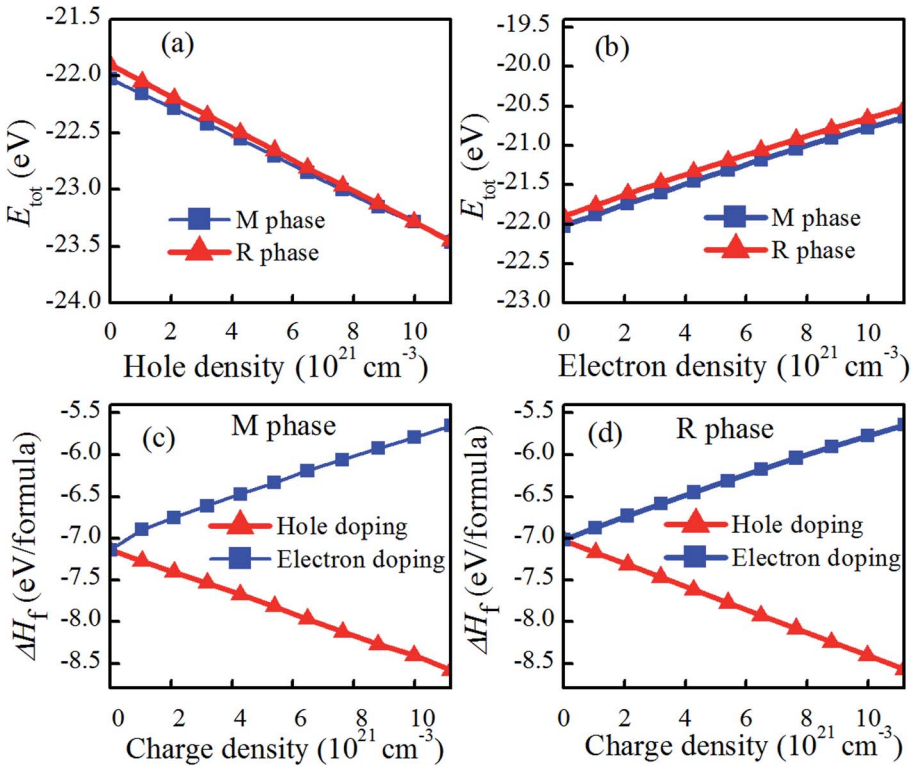

Fig. 2 Total energies (E_{tot}) of charge doping in M and R phase as a function of charge density, and formation energy of charge doped VO_2. (a) Hole doping, (b) electron doping, (c) charge doped VO_2(M), and (d) charge doped VO_2(R).

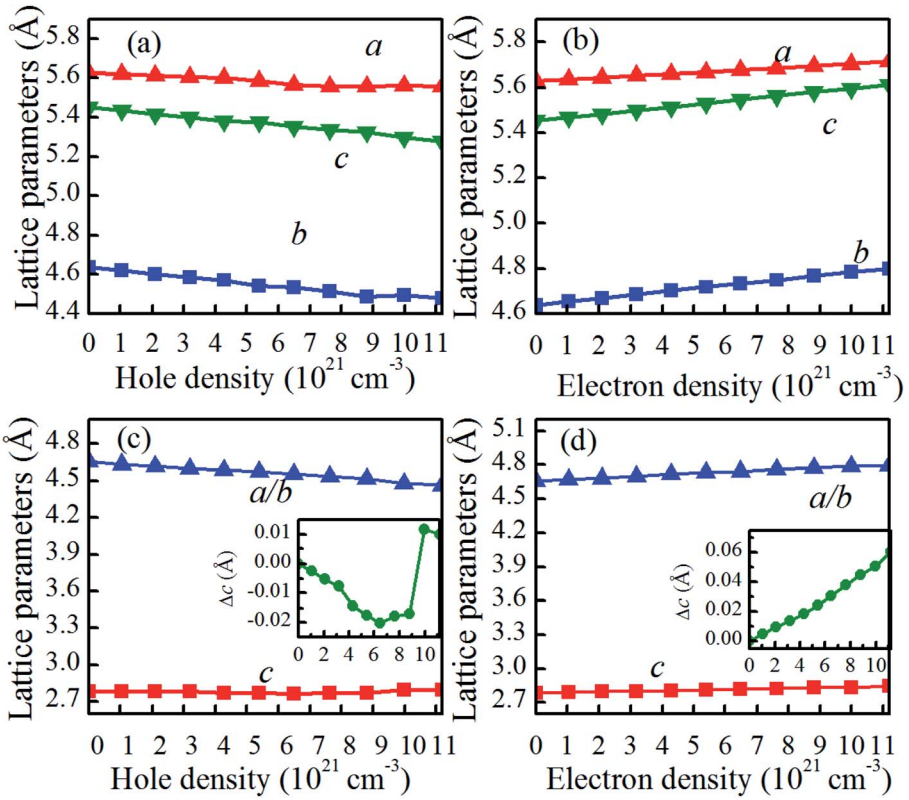

Fig. 4 Lattice parameters of (a) hole or (b) electron doped VO_2(M), and (c) hole or (d) electron doped VO_2(R). The inset figure is the variation of c, *i.e.*, Δc ($c - c_0$). The c and c_0 are the supercell lengths along the c-axis at equilibrium and charge-doped VO_2.

3.2 Atomic and electronic structures of charge-doped VO_2

The reduction in T_c for charge-doped VO_2 should be coupled with the changes in the atomic and electronic structure, as discussed in the next section. For charge-doped VO_2(M), as shown in Fig. 4(a and b), the lattice parameters b and c of are slightly increase, and the lattice parameter a remains nearly unchanged under the considered electron density. However, these parameters (a, b, c) slightly decrease with increasing of hole density. This outcome further confirms that the reduction in the T_c in hole doped VO_2 is due to the shorter a-axis length.[33,34] Moreover, the lattice parameter a expressing the V–V chains promotes the transition from the monoclinic phase to the rutile phase at a lower temperature than that of pristine VO_2. Applying the compression strain along the a-axis balances the V–V distance. In addition, applying the compression strain along the a-axis results in the overlapping of d orbitals, which increases the d bandwidth and then forces it to transition from the monoclinic phase to the rutile phase, thus causing the reduction in T_c. Experimentally, Fan *et al.* reported that stretching of a-axis will increase the T_c of VO_2 films.[33] Muraoka *et al.* found that the appearance strain along the a-axis from VO_2/TiO_2 thin films has a large influence on the MIT of VO_2.[34] Therefore, hole doping in the concentration range considered is able to promote the phase transition in VO_2. The opposite is true for electron doping. For charge-doped VO_2(R), as shown in Fig. 4(c and d), the c axis is slightly shorten, and then slightly elongated in the hole-doping VO_2(R), while the c axis is slightly elongated in electron-doping VO_2(R). This may attribute the fact that the charge-injection would induce variable orbital occupancy, which is similar to the experimental results.[19]

It is reported that the V–V chains are one of the key characteristics of VO_2 in determining the atomic and electronic properties at different phases.[35,36] As shown in Fig. 1, in pristine VO_2(R), all the V atoms arrange uniformly along the c axis with nearest-neighbor V–V distances of 2.788 Å. However, pristine VO_2(M) exhibits Peierls distortion in the V–V chains along the a-axis, in which the short and long V–V bonds (2.520 Å *vs.* 3.143 Å) are arranged alternately. Compared with those of pristine VO_2(M), as shown in Fig. 5(a and b), the short and long V–V bond distances are nearly unchanged and still maintain the dimerization characteristics after electron doping. However, hole doping results in a gradual shortening of the long V–V bond distances and a gradual elongation of the short V–V bond distances below a critical hole density of 6.48×10^{21} cm^{-3}. This phenomenon could also be observed experimentally in the intermediate phase of VO_2(M2), in which only half of the V atoms are dimerized, while the other half form chains of is equally spaced atoms.[37] Once above the critical hole density, the alternatively short and long V–V bond distances jump, and the equidistant V–V bond distances (2.7–2.8 Å) are similar to the V–V bond length in VO_2(R) (as shown in Fig. 5(a)). These results indicate that VO_2 transits from the monoclinic phase to the rutile phase within the range of a certain hole-doping density. Yuan *et al.* proved that the appearance of this phenomenon is

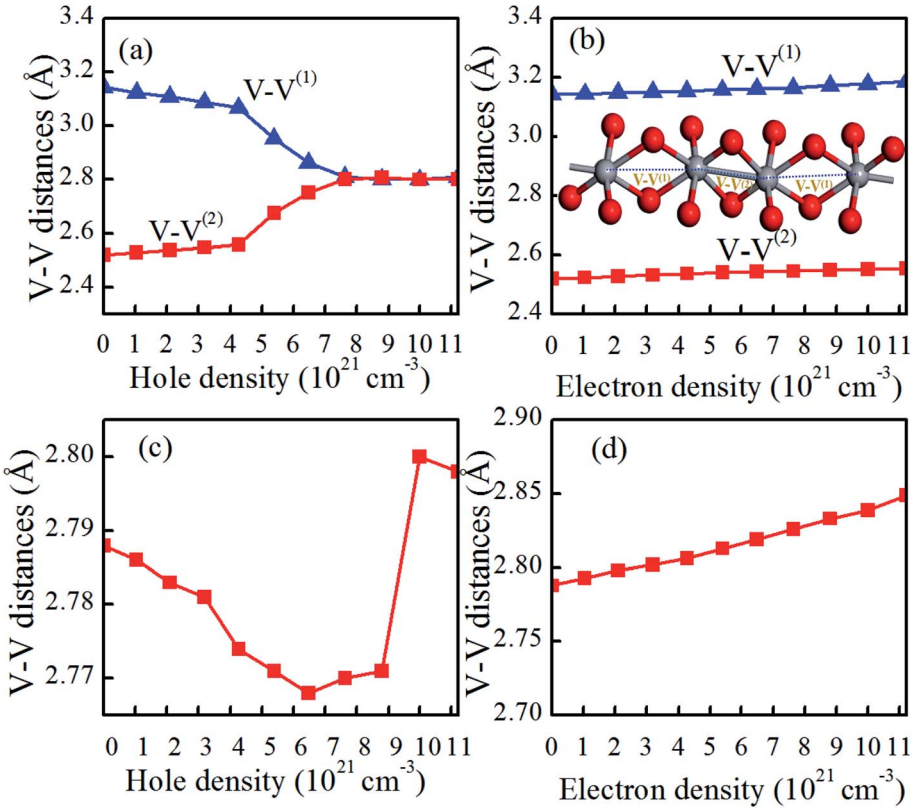

Fig. 5 Dependence of V–V distances in (a) hole or (b) electron doped VO_2(M) and (c) hole or (d) electron doped VO_2(R) on the charge-doping density. The long V–V bonds denote V–$V^{(1)}$, and the short V–V bonds denote V–$V^{(2)}$. The inserted figure shows the V–V bonds in the VO_2(M). The V and O atoms are indicated by the gray and red spheres, respectively.

attributed to a strong lattice-hole coupling.[38] Experimentally, it is found that a critical hole density induces a sudden rapidly variable V–V bond, which is related to the critical excitation influence.[39–42] As shown in Fig. 5(c), the V–V distances in the hole-doping VO_2(R) has a very fast change into alternatively short and long bond distances, for the V–V chains. In contrast, as shown in Fig. 5(d), the V–V distances in electron-doping VO_2(R) seem slightly to increase. Therefore, it can be concluded that the hole-injection has greater influence on the V–V bond lengths than the electron-injection in VO_2.

The structural transition in VO_2 is accompanied by changes in the electronic band structure near the Fermi level that can be qualitatively understood within a crystal field model.[31] As shown in Fig. 6(a), the twisting of the V–V chains causes splitting of the $d_{\|}$ orbital into filled bonding and empty antibonding orbitals, while making the π^* orbital move to a higher energy level, thus opening the band gap. Actually, the VO_2 phase transition is relative to the octahedral environment and the associated hybridization of the O-2p orbitals with the V-3d orbital.[31] As shown in Fig. 6(b), for VO_2(M), each VO_6 octahedron shares edges with its neighboring octahedra, forming chains along the *a*-axis. In addition, the V-3d orbitals split into a combination of low-energy states and high-energy states, where the high-energy states involve the symmetry of the V–O bonds. In charge-doping VO_2(M), as shown in Fig. 6(c and d), the V–O distance is slightly lengthened with the increase in electron density, and could further decrease the p–d overlap.[43] The increase in the V–O bond results in the expansion of the lattice volume due to the decrease in c_R/a_R and further induces the reduction in T_c.[43] Therefore, we can conclude that electron doing makes the V–O bond length longer and thus reduces the T_c in VO_2. However, as the hole density increases, the V–O bond lengths are gradually reduced. When the hole density reaches 5×10^{21} cm^{-3}, d_2 experiences a dramatic increase, and d_5 decreases sharply, which will increase the p–d overlap, and thus both the $d_{\|}$ and π^* orbitals are partially occupied at Fermi level.[43] This phenomenon confirms that VO_2 may experience a metal–insulator transition.

As shown in Fig. 6(e), in the VO_2(R), the apical and equatorial V–O bond lengths increase with the increase of electron density, which is due to the decrease in the ration of *c*/*a*. However, as shown in Fig. 6(f), the apical and equatorial V–O bond lengths decrease with the increase hole density.

Except for the variable V–O bond, the band gap evolution of charge-doped VO_2 is related to the atomic structure change described by the V–V chains and twisting angle δ and the electronic structure change described by orbital switching. As shown in Fig. 7(a and b), δ in the V–V chains of electron-doped VO_2 tends to gradually decrease, indicating that the V–V bond characterizes a dimerizing feature. However, when the hole density is from 0 to 4.28×10^{21} cm^{-3}, δ in the V–V chains decreases monotonically, as the hole density increase further, the value of δ sharply decreases, finally reaching zero, which

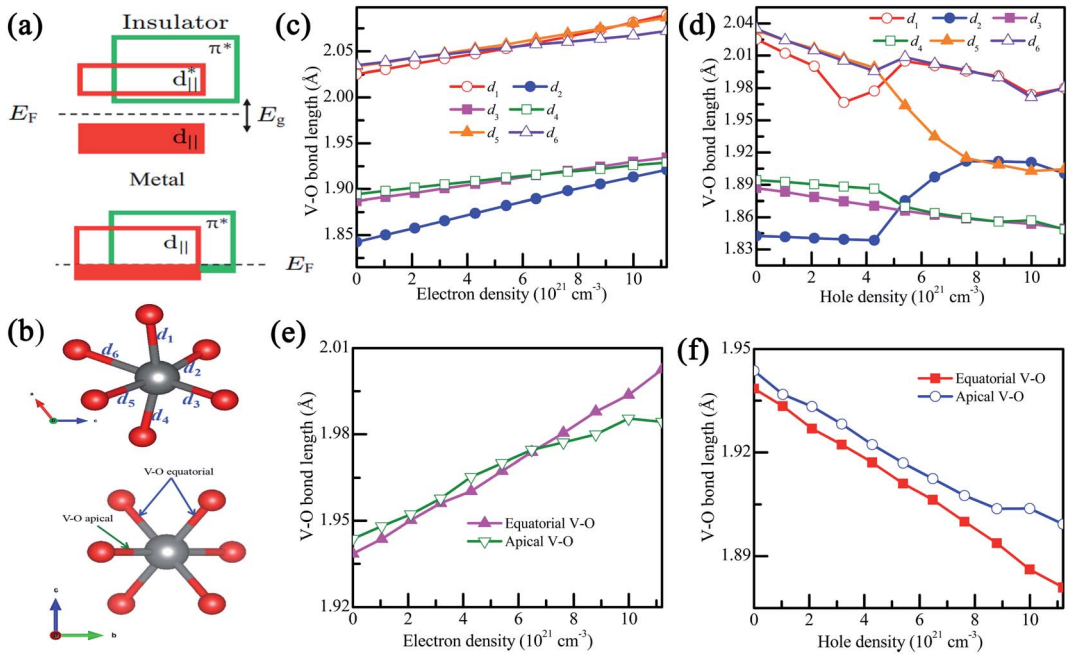

Fig. 6 (a) Bandwidth scheme of pristine VO_2, (b) an octahedron at the center of VO_2, (c and d) the V–O bond lengths in charge doped VO_2(M), and (e and f) the V–O bond lengths in hole-doped VO_2(R). The bond distances in VO_2(M) are d_1, d_2, d_3, d_4, d_5 and d_6. The bond lengths in VO_2(R) are the equatorial and apical V–O.

demonstrates that the alternatively short and long V–V bond distances in VO_2(M) quickly change into equal V–V bonds. In addition, the average twisting angle δ in the V–V chains exhibits excellent consistency with the band gap change of VO_2 from R to M1. As in Gao's previous discussion,[35] the significant dimerization in V–V, slight twisting of δ or the variable V–O bond can

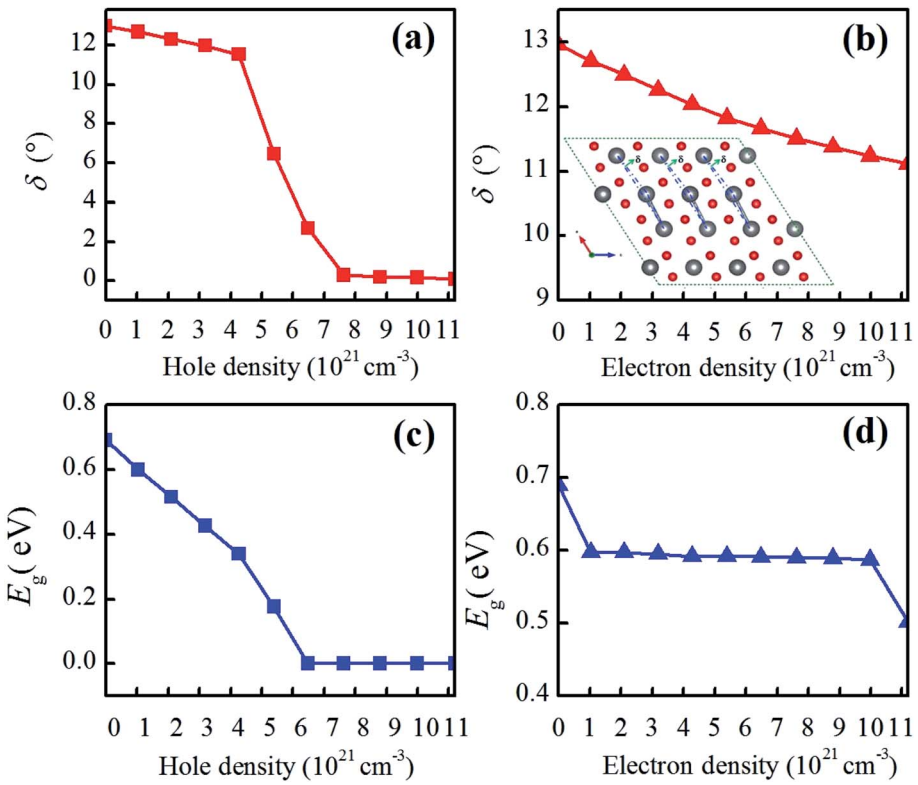

Fig. 7 (a and b) Average twisting angle (δ) of the V–V chains and (c and d) the band gaps in charge-doped VO_2(M). (a and c) Electron doping, and (b and d) hole doping. The inserted figure in (b) is the δ angle in the V–V chains in VO_2(M).

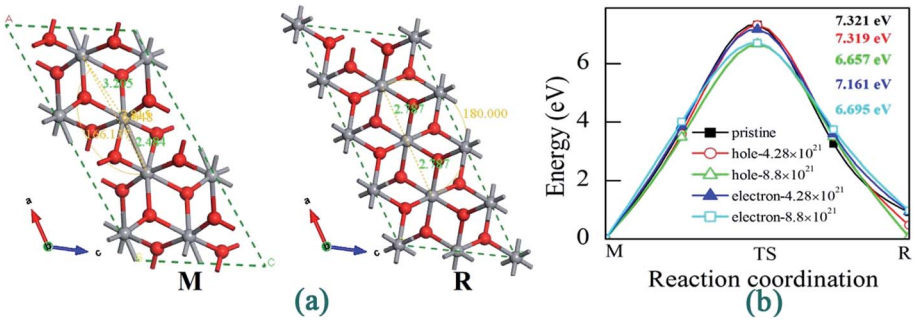

Fig. 8 (a) Structures of VO_2 (M/R) and (b) energy barriers from M to R phase under different charge doping.

be regarded as the characteristic parameters of the structure-driven transition. As shown in Fig. 7(c), when the hole density is increased by 5.4 × 10^{21} cm^{-3}, the band gaps of VO_2(M) linearly decrease and eventually decrease to 0 eV with the increase in hole density. The band gap undergoes a fast change, and exhibits a similar change tendency as the twisting angle δ. This phenomenon is consistent with the other result calculated from Lee *et al.*,[14] who reported that VO_2 exhibits a significant band-gap narrowing for a charge concentration from 0.025 to 0.5 hole/electron per VO_2. Experimentally, Zhang *et al.* found that N atoms-substituted O atoms induce narrowing of the energy band gap due to weakening of the interaction within the V–V dimer with the hole injected into the $d_{||}$ sub-bands.[18] In contrast, as shown in Fig. 7(d), as the electron density increases from 0 to 1.2 × 10^{22} cm^{-3}, the band gaps of VO_2(M) experience a slight reduction ranging from 0.69 eV to 0.502 eV. Apparently, electron doping induces a slow MIT, and its density has some effect on the phase transition. Theoretically, a fascinating rebound behavior of the transition temperature is observed. By increasing the doping concentration of W into VO_2, the MIT is tuned to a lower temperature at the beginning and then anomalously shifted to a higher temperature.[44]

In order to reveal the kinetic limit for charge-driven phase transition in VO_2, we performed CINEB calculations to obtain the phase transition barriers. As shown in Fig. 8(a), we redefined the lattice parameters for VO_2(R) from tetragonal and monoclinic view to better reveal the kinetic limit for charge-driven phase transition in VO_2 (As listed in Table 2). Fig. 8(b) shows the energy curves of M-to-R phase transition in pristine and charge-doping VO_2 with certain density. It can be found that the energy barriers are too higher for VO_2 transiting from M phase to R phase, indicating that it requires additional conditions to drives the M-to-R phase transition, such as the temperature, pressure and light radiation.[32]

To elucidate the possible driving forces behind the MIT, we further calculated the total and partial densities of states (DOSs) of charge-doped VO_2(M). As shown in Fig. 9(a), for pristine VO_2(M), the electrons around E_F occupy the t_{2g}-state $d_{x^2-y^2}$ orbital (π), while the conduction is mainly occupied by the e_g-state d_{z^2} orbital (σ). At hole densities of 2.1 × 10^{21} cm^{-3} and 4.28 × 10^{21} cm^{-3}, the band gaps of VO_2(M) are reduced to 0.515 eV and 0.34 eV, respectively. Near the E_F, the electrons dominantly occupy the $d_{x^2-y^2}$ orbital and d_{yz} orbital. In contrast, fewer electrons occupy the d_{z^2} orbital (σ). More importantly, this electronic structure characteristic remains from 0 to 6.48 × 10^{21} cm^{-3} (the critical hole density). Interestingly, when the hole density reaches the critical hole density, VO_2 exhibits metallic properties, as shown in Fig. 9(d). There is a strong interaction near the Fermi level between the $d_{x^2-y^2}$ and d_{z^2} orbitals. This result is also consistent with the previous discussion on the significant dimerization in V–V and a slight twisting of δ, which could be regarded as the characteristic parameters of the structure-driven transition. However, from Fig. 9(e–h), the Fermi levels are shifted into the conduction band to varying degrees with the increase in electron doping. The states near the Fermi level are mainly occupied by the d_{z^2} orbital, while the valence bands mainly consist of the $d_{x^2-y^2}$ orbital. Furthermore, it can be observed that the electronic structure of VO_2 changes slightly for different electron concentrations. More importantly, although there are some changes in the band gap from 0.597 eV to 0.502 eV and the location of E_F, this electronic structure characteristic remains as electron doping increases. Therefore, it can be concluded that the band gap of VO_2 with charge doping should be attributed to an electron-correction-driven Mott transition in which orbital switching occurs between the $d_{x^2-y^2}$ and d_{z^2} states. Experimentally, by soft-X-ray absorption spectroscopy, orbital-assisted MIT is also observed in VO_2.[43]

Fig. 10 shows the density of states of pure VO_2(R) and charge-doping VO_2(R). It is seen that pristine VO_2(R) and charge-doped VO_2(R) exhibit metallic properties as the Fermi level crosses the conduction band. Furthermore, electrons around Fermi level mainly occupy the $d_{x^2-y^2}$ orbital and d_{z^2} orbital. In addition, as the hole density increases, the former has a higher occupant than the latter. However, as the electron density increases, the occupant of d_{z^2} orbital is higher than that of the $d_{x^2-y^2}$ orbital. In

Table 2 Calculated lattice parameters for VO_2 (M/R)

VO_2	a (Å)	b (Å)	c (Å)	α (deg)	β (deg)	γ (deg)	Ref.
R	4.609	4.609	2.785	90	90	90	35
Monoclinic R	5.575	4.653	5.427	90	120.936	90	This calc.
M	5.610	4.571	5.393	90	121.9	90	35
M	5.648	4.634	5.450	90	121.64	90	This calc.

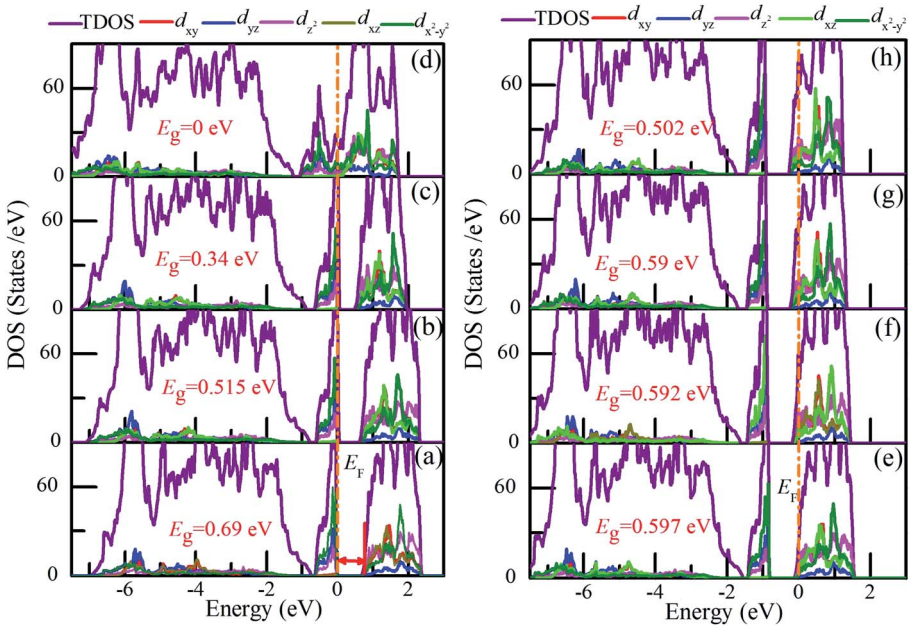

Fig. 9 Total and projected density of states (DOS) of (b–d) hole-doped and (e–h) electron-doped VO_2(M). The concentrations of charge are (a) pristine, (b) 2.1×10^{21} cm^{-3}, (c) 4.28×10^{21} cm^{-3}, (d) 8.8×10^{21} cm^{-3}, (e) 1.04×10^{21} cm^{-3}, (f) 4.28×10^{21} cm^{-3}, (g) 7.63×10^{21} cm^{-3}, and (h) 1.12×10^{22} cm^{-3}. The Fermi level (E_F) is set to 0 eV.

general, there is a significant orbital switching between the $d_{x^2-y^2}$ and d_{z^2} orbitals accompanied by obvious V–V dimerization and a slight twisting of δ in the charge-doped VO_2.

3.3 Discussion

Charge-doping greatly impacts on the atomic and electronic structures of VO_2. From the Fig. 3, it is found that the charge-doping including hole and electron-doping could trigger the phase transition of VO_2. More interestingly, the effect of hole doping on the T_c is greater than that of electron-doping. This is consistent with other calculation result. As is predicted by Zhang *et al.*, the hole doping was superior to electron doping for modulating the phase transition of VO_2.[38] From a geometric viewpoint, the octahedra in VO_2 are orthorhombically distorted, making it possible to differentiate the V–O bonds. After electron-doping, the V–O bond length change significantly in

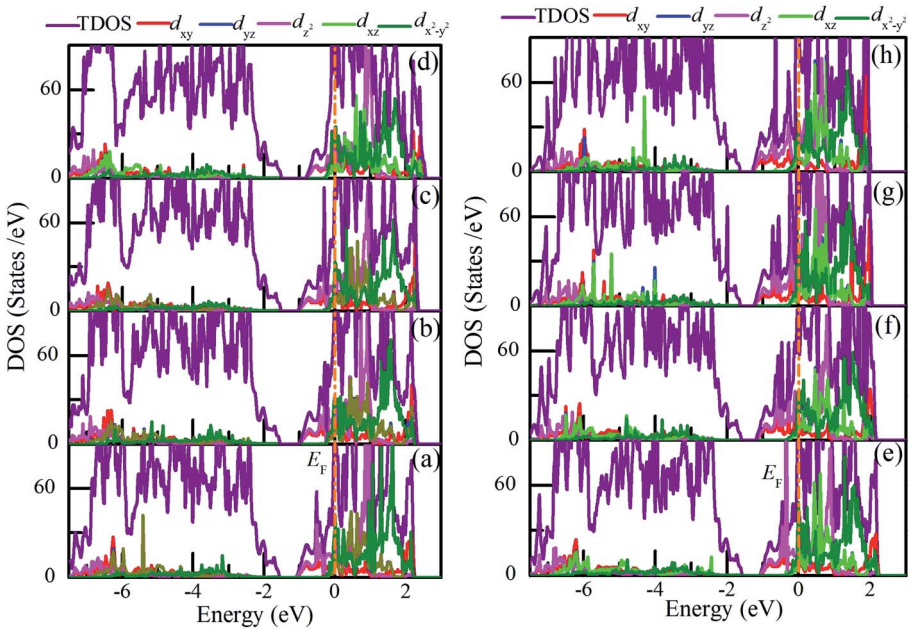

Fig. 10 Total and projected density of states (DOS) of (b–d) hole-doped and (e–h) electron-doped VO_2(R). The concentrations of charge are (a) pristine, (b) 2.1×10^{21} cm^{-3}, (c) 4.28×10^{21} cm^{-3}, (d) 8.8×10^{21} cm^{-3}, (e) 1.04×10^{21} cm^{-3}, (f) 4.28×10^{21} cm^{-3}, (g) 7.63×10^{21} cm^{-3}, and (h) 1.12×10^{22} cm^{-3}. The Fermi level (E_F) is set to 0 eV.

VO_2(R). However, for hole-doping, the alternatively short and long V–V bond distances has very fast change into the equidistant V–V bond in VO_2(M). Furthermore, the twisting angle δ experiences a great change. These phenomena are ascribed to structure-driven transition due to the large δ and V–V bond length change.[35] From the electronic structure viewpoint, the characteristic of VO_2 transition from the semiconducting state to the metallic state appears due to the strong interaction between the $d_{x^2-y^2}$ and d_{z^2} orbitals near the Fermi level, which can be attributed to the electron-driven the transition. Therefore, it can be concluded that charge-doping may provide an efficient way to modulate the MIT in VO_2.

4. Conclusions

In summary, we performed first-principles calculations to investigate the behavior of charge doping and its influence on the phase transition temperature of VO_2. Charge doping could effectively modulate the T_c, assisting the VO_2 phase transition at room temperature. Hole doping induces a significant band-gap narrowing with increasing of hole concentration. The characteristic VO_2 transition from the semiconducting state to the metallic state appears once above the critical hole density (6.48×10^{21} cm^{-3}), which is due to the strong interaction between the $d_{x^2-y^2}$ and d_{z^2} orbitals near the Fermi level. However, electron doping shows a slight band-gap narrowing with increasing electron concentration. The V–O bond lengths significantly increase. The results will provide insights into phase transitions of VO_2 thermochromic materials across the MIT suitable for applications such as smart windows.

Conflicts of interest

There are no conflicts to declare.

Acknowledgements

The authors gratefully acknowledge support from the National Natural Science Foundation of China (51873102, 51972206), the Open Project Fund of Key Laboratory for Optoelectronics and Communication of Jiangxi Province (20181OEC001), the School-level Scientific Research Project of Hubei Polytechnic University (18xjz11R), and the Innovation Training Program of Hubei Province (S201910920031). The computation was conducted using the high performance computing platform of Shanghai University.

References

1 F. J. Morin, *Phys. Rev. Lett.*, 1959, **3**, 34–36.
2 C. Granqvist, *Phys. Scr.*, 1985, **32**, 401–407.
3 T. Driscoll, H. Kim, B. Chae, M. Ventra and D. Basov, *Appl. Phys. Lett.*, 2009, **95**, 043503.
4 B. Kim, Y. Lee, B. Chae, S. Yun, S. Oh, H. Kim and Y. Lim, *Appl. Phys. Lett.*, 2007, **90**, 023515.
5 L. Kang, Y. Gao, H. Luo, J. Wang, B. Zhu, Z. Zhang, J. Du, M. Kanehira and Y. Zhang, *Sol. Energy Mater. Sol. Cells*, 2011, **95**, 3189–3194.
6 Y. Gao, S. Wang, H. Luo, L. Dai, C. Cao, Y. Liu, Z. Chen and M. Kanehira, *Energy Environ. Sci.*, 2012, **5**, 6104–6110.
7 Y. Cui, Y. Ke, C. Liu, Z. Chen, N. Wang, L. Zhang, Y. Zhou, S. Wang, Y. Gao and Y. Long, *Joule*, 2018, **2**, 1707–1746.
8 C. Tang, P. Georgopoulos, M. E. Fine, J. B. Cohen, M. Nygren, G. S. Knapp and A. Aldred, *Phys. Rev. B: Condens. Matter Mater. Phys.*, 1985, **31**, 1000–1011.
9 L. Chen, Y. Liu, K. Yang, P. Lan, Y. Cui, H. Luo, B. Liu and Y. Gao, *Comput. Mater. Sci.*, 2019, **161**, 415–421.
10 L. Chen, Y. Cui, S. Shi, B. Liu, H. Luo and Y. Gao, *RSC Adv.*, 2016, **6**, 86872.
11 S. Zhang, I. S. Kim and L. J. Lauhon, *Nano Lett.*, 2011, **11**, 1443–1447.
12 J. P. Pouget, H. Launois, J. P. D'haenens, P. Merenda and T. M. Rice, *Phys. Rev. Lett.*, 1975, **35**, 873–875.
13 J. Jeong, N. Aetukuri, T. Graf, T. D. Schladt, M. G. Samant and S. S. P. Parkin, *Science*, 2013, **339**, 1402–1405.
14 D. Lee, B. Chung, Y. Shi, G. Y. Kim, N. Campbell, F. Xue, K. Song, S. Choi, J. Podkaminer, T. Kim, P. Ryan, J. Kim, T. Paudel, J. Kang, J. Spinuzzi, D. Tenne, E. Tsymbal, M. Rzchowski, L. Chen, J. Lee and C. Eom, *Science*, 2018, **362**, 1037.
15 J. Zhang, H. He, Y. Xie and B. Pan, *Phys. Chem. Chem. Phys.*, 2013, **15**, 4687.
16 K. Wang, W. Zhang, L. Liu, P. Guo, Y. Yao, C. Wang, C. Zou, Y. Yang, G. Zhang and F. Xu, *Appl. Surf. Sci.*, 2018, **447**, 347–354.
17 M. Wan, M. Xiong, N. Li, B. Liu, S. Wang, W. Ching and X. Zhao, *Appl. Surf. Sci.*, 2017, **410**, 363–372.
18 W. Zhang, K. Wang, L. Fan, L. Liu, P. Guo, C. Zou, J. Wang, H. Qian, K. Ibrahim, W. Yan, F. Xu and Z. Wu, *J. Phys. Chem. C*, 2014, **118**, 12837–12844.
19 L. Dai, S. Chen, J. Liu, Y. Gao, J. Zhou, Z. Chen, C. Cao, H. Luo and M. Kanehira, *Phys. Chem. Chem. Phys.*, 2013, **15**, 11723–11729.
20 M. Wan, B. Liu, S. Wang, L. Hu, H. Tao and X. Zhao, *J. Alloys Compd.*, 2017, **706**, 289–296.
21 T. Hajlaoui, N. Émond, C. Quirouette, B. L. Drogoff, J. Margot and M. Chaker, *Scr. Mater.*, 2020, **177**, 32–37.
22 J. Zhang, H. He, Y. Xie and B. Pan, *J. Chem. Phys.*, 2013, **138**, 114705.
23 V. Andreev, V. M. Kapralova and V. Klimov, *Phys. Solid State*, 2007, **49**, 2318–2322.
24 G. Kresse and J. Hafner, *Phys. Rev. B: Condens. Matter Mater. Phys.*, 1993, **47**, 558–561.
25 G. Kresse and J. Furthmuller, *Phys. Rev. B: Condens. Matter Mater. Phys.*, 1996, **54**, 11169–11186.
26 J. P. Perdew, K. Burke and M. Ernzerhof, *Phys. Rev. Lett.*, 1996, **77**, 3865–3868.
27 P. E. Blochl, *Phys. Rev. B: Condens. Matter Mater. Phys.*, 1994, **50**, 17953–17979.
28 S. L. Dudarev, G. A. Botton, S. Y. Savrasov, C. J. Humphreys and A. P. Sutton, *Phys. Rev. B: Condens. Matter Mater. Phys.*, 1998, **57**, 1505–1509.

29 L. Chen, A. Wang, Z. Xiong, S. Shi and Y. Gao, *Appl. Surf. Sci.*, 2019, **467–468**, 22–29.
30 M. Netsianda, P. E. Ngoepe, C. Richard, A. Catlow and S. M. Woodley, *Chem. Mater.*, 2008, **20**, 1764–1772.
31 J. Goodenough, *J. Solid State Chem.*, 1971, **3**, 490–500.
32 X. Zhou, H. Shu, Q. Li, P. Liang, D. Cao and X. Chen, *J. Mater. Chem. C*, 2020, **8**, 4432–4440.
33 L. Fan, S. Chen, G. Liao, Y. Chen, H. Ren and C. Zou, *J. Phys.: Condens. Matter*, 2016, **28**, 255002.
34 Y. Muraoka, Y. Ueda and Z. Hiroi, *J. Phys. Chem. Solids*, 2002, **63**, 965–967.
35 S. Chen, J. Liu, H. Luo and Y. Gao, *J. Phys. Chem. Lett.*, 2015, **6**, 3650–3656.
36 T. Yao, X. Zhang, Z. Sun, S. Liu, Y. Huang, Y. Xie, C. Wu, X. Yuan, W. Zhang, Z. Wu, G. Pan, F. Hu, L. Wu, Q. Liu and S. Wei, *Phys. Rev. Lett.*, 2010, **105**, 226405.
37 Y. Ji, Y. Zhang, M. Gao, Z. Yuan, Y. Xia, C. Jin, B. Tao, C. Chen, Q. Jia and Y. Lin, *Sci. Rep.*, 2014, **4**, 4854.
38 X. Yuan, W. Zhang and P. Zhang, *Phys. Rev. B: Condens. Matter Mater. Phys.*, 2013, **88**, 035119.
39 C. Kübler, H. Ehrke, R. Huber, R. Lopez, A. Halabica, R. F. Haglund and A. Leitenstorfer, *Phys. Rev. Lett.*, 2007, **99**, 116401.
40 P. Baum, D. S. Yang and A. H. Zewail, *Science*, 2007, **318**, 788.
41 S. Wall, D. Wegkamp, L. Foglia, K. Appavoo, J. Nag, R. F. Haglund, J. Stähler and M. Wolf, *Nat. Commun.*, 2012, **3**, 721.
42 D. Hilton, R. Prasankumar, S. Fourmaux, A. Cavalleri, D. Brassard, M. Khakani, J. Kieffer, A. Taylor and R. Averitt, *Phys. Rev. Lett.*, 2007, **99**, 226401.
43 N. Aetukuri, A. Gray, M. Drouard, M. Cossale, L. Gao, A. Reid, R. Kukreja, H. Ohladag, C. Jenkins, E. Arenholz, K. Roche, H. Dürr, M. Samant and S. Parkin, *Nat. Phys.*, 2013, **9**, 661–666.
44 M. Nisar, Z. Lin, G. Xu, Y. Liu and G. Han, *J. Appl. Phys.*, 2019, **126**, 195106.

